A numerical model of delamination in composite laminated beams using the LRZ beam element based on the refined zigzag theory

CrossMark

A. Eijo *, E. Oñate, S. Oller

International Center for Numerical Methods in Engineering (CIMNE), Universitat Politècnica de Catalunya (UPC), Campus Norte UPC, 08034 Barcelona, Spain

A R T I C L E   I N F O

A B S T R A C T

A method based on the Refined Zigzag Theory (RZT) to model delamination in composite laminated beam structures is presented. The novelty of this method is the use of one-dimensional finite elements to discretize the geometry of the beam. The key property of this beam element, named LRZ [1], is the possibility to capture the relative displacement between consecutive layers which occurs during delamination. The fracture mode that the LRZ element is capable to predict is mode II. In order to capture the relative displacement using the LRZ element it is necessary to adapt the RZT theory as presented in this paper. The mechanical properties of the layers are modeled using a continuum isotropic damage model [2]. The modified Newton–Raphson method is used for solving the non-linear problem.

The RZT theory, the LRZ finite element and the isotropic damage model are described in the paper. Also, the implicit integrations algorithm is presented. The performance of the LRZ element is analyzed by studying the delamination in a beam for two different laminates, using the plane stress solution as a reference.

© 2013 Elsevier Ltd. All rights reserved.

1. Introduction

Delamination, i.e. interlaminar cracks, is a common and dangerous source of damage in laminated composite materials [3] characterized by the loss of adherence between the different plies of the laminate. This phenomenon can occur during the fabrication stage or during the transportation, storage and service phases. Imperfection of various natures and thermal and chemical shrinkage of components may produce delamination during the manufacturing process. Many causes such as local forces, thermal actions and low energy impacts may serve as sources of delamination during the transportation, storage or service period. Geometry discontinuities such as access holes, notches, free edges or bonded and bolted joints can also produce delamination due to high stress gradients. Once delamination occurs, the structural member considerably reduces its original stiffness, which leads to its failure in conjunction with other mechanic phenomena, e.g. buckling, excessive vibration or loss of fatigue life.

Within the framework of numerical simulation, delamination is usually modeled using fracture or damage mechanics procedures. In fracture mechanics, the virtual crack closure technique (VCCT) [4,5] is the most widely used approach, which is based on the assumption that the energy necessary to open the crack is the same to close it. Damage mechanics is based on the concept of a cohesive damage zone developed near the crack front, where the stresses are limited by the yield stress and a thin plastic zone is generated in front of the crack. This technique can easily be implemented in the finite element method leading to cohesive finite elements [6–10].

Each of these techniques has their own drawbacks. One of the most significant is that it is necessary to place interface cohesive or fracture finite elements between the plies where delamination is expected to occur. If the delamination path is unknown, interface finite elements must be placed between all plies. This typically leads to an unbearable computational cost depending on the number of physical composite layers and on the structure size. In order to overcome this problem, Martinez et al. [11] proposed to study delamination under the continuum mechanics setting using a 3D finite element method and an isotropic damage model which manages material degradation.

The efficacy of all above mentioned techniques is undisputed. However, the use of 3D finite elements for discretizing the geometry considerably increases the computational costs and storage, specially for non-linear problems. Surely, there are several cases, for instance: delamination in bonded joints, where 3D finite element analysis is indispensable. However, it is practically impossible to use these methods in large laminated composite structures with tens of layers, e.g. wind turbine blades or aircraft fuselage in composite materials, where simpler models should be used.

Classical thin beam/plate theory [12,13] and the more advanced First Order Shear Deformation Theory (FSDT) [14–16] were the first simplified theories capable to precisely model a plate structure of

* Corresponding author. Tel.: +34 934010808.
 E-mail address: aeijo@cimne.upc.edu (A. Eijo).

homogeneous material. However, when applied to highly heterogeneous laminated composite materials it is known that both theories give poor predictions. The cause of this drawback is that these theories propose a linear thickness distribution of the axial displacement, which is unable to represent the complex real kinematics of a laminated composite. Because of the same reason, both theories are unable to predict delamination, as they cannot capture the relative displacement between two consecutive layers.

More accurate models are based on Layer–Wise theories (LWTs) [17–19] in which the thickness coordinate is divided into a number of analysis sublayers (that may be not coincident with the number of physical layers), assuming a separate displacement field within each ply and forcing displacement constraints and stress contact conditions at the interfaces. LWT are able to capture accurately interlaminar stresses directly from the constitutive equations. Also, these theories are capable to simulate the delamination phenomenon [20–24] due to the high level of refinement of the displacement field. However, since the number of unknowns is proportional to the number of analysis sublayers, the computational cost increases with the number of subdivisions.

ZigZag (ZZ) theories are an attractive compromise between the high accuracy of LWT and the computational efficiency of FSDT [19,25,26]. In ZZ theories the in-plane displacement is modeled by a superposition of a piecewise linear displacement functions (the zigzag function) over a linear, quadratic or cubic displacement field along the thickness direction. An important property of ZZ theories is that the number of kinematics variables is independent of the number of layers. Although many ZZ theories require C^1 continuity for the deflection field, which is a disadvantage versus simpler C^0 continuity plate theories, some evolved ZZ techniques [27,28] have been developed to overcome this shortcoming. However, several C^0 continuous ZZ formulations for beams suffer from their inability to model correctly a clamped boundary condition, which makes it difficult to satisfy equilibrium of forces at a support. So far, the use of the ZZ theories to model delamination in beams and plates has been quite limited. A C^0 plate element for delamination analysis based on a ZZ model has been developed by Icardi and Zardo [29].

Tessler et al. [30–32] have developed an improved ZZ model for beams and plates, called *Refined ZigZag Theory* (RZT), that adopt FSDT displacement fields as the baselines. The key attributes of the RZT are, first, the proposed linear piecewise zigzag function vanishes at top and bottom surfaces of the structural section. Second, it does not require full transverse shear stress continuity across the laminated. Third, C^0 continuity is only required for the *finite element method* (FEM) approximation of the kinematic variables and finally, all boundary conditions, including the fully clamped condition, can be simulated effectively. Oñate et al. [1] have taken the RZT as the basis for developing a simple two-noded linear C^0 beam element named LRZ. The accuracy of the LRZ beam element for analyzing composite laminated beams has been demonstrated for simple support and clamped boundary conditions under different loads. Oñate et al. [1] have also shown that the LRZ element is capable to capture the relative displacement between layers, typical of a delamination process. It is necessary to mention however that this element can only model the fracture mode II.

In this paper we exploit the capabilities of the RZT element to model delamination (mode II) in laminated beams using an isotropic damage model [2,33] for modeling the nonlinear material behavior. The paper layout is the following. A brief description of the RZT theory, the LRZ finite elements and the isotropic damage model are presented first. Then, the implicit integration algorithm is shown. The non-linear problem is solved by the modified Newton–Raphson method. Finally, the performance of the LRZ element is shown by modeling delamination in a beam for two different laminates, where the reference solution is a plane stress analysis.

2. Refined Zigzag Theory (RZT) for beams and LRZ beam element

2.1. RZT kinematics

Consider a composite laminated beam of depth b, thickness h, and length L, formed by N layer of thickness h^k. The reference coordinate system is the 2D Cartesian system (x, z), where x is set as the in-plane coordinate and z is the thickness coordinate.

The displacement field assumed in the linear piecewise zigzag RZT is written as

$$u^k(x,z) = u_0(x) - z \cdot \theta(x) + \bar{u}^k(x,z)$$
$$w(x) = w_0(x) \tag{1a}$$

In Eq. (1a) the zigzag displacement function $\bar{u}^k$ is expressed as

$$\bar{u}^k = \phi^k(z) \cdot \psi(x); \quad k = 1, N \tag{1b}$$

where superscript k indicates quantities within the kth layer with $z_k \leqslant z \leqslant z_{k+1}$, and z_k is the vertical coordinate of the kth interface; ψ is a primary kinematic variable defining the amplitude of the zigzag function on the beam and ϕ^k is a known piecewise linear zigzag function. u_0 is the uniform axial displacement along the beam axis direction x; θ represents the anticlockwise rotation of the normal and w_0 is the *deflection*.

The kinematics variables are

$$\mathbf{a} = [u_0 \quad w_0 \quad \theta \quad \psi]^T \tag{2}$$

The in-plane ε^k and the transverse shear γ^k strains are defined as

$$\varepsilon^k = \frac{\partial u^k}{\partial x} = \frac{\partial u_0}{\partial x} - z \cdot \frac{\partial \theta}{\partial x} + \phi^k(z) \cdot \frac{\partial \psi}{\partial x}$$
$$\gamma^k = \frac{\partial u^k}{\partial z} + \frac{\partial w}{\partial x} = \gamma(x) + \beta^k \cdot \psi(x) \tag{3}$$

which can be written in matrix form as

$$\boldsymbol{\varepsilon}^k = \begin{bmatrix} \varepsilon^k \\ \gamma^k \end{bmatrix} = \begin{bmatrix} 1 & -z & \phi^k & 0 & 0 \\ 0 & 0 & 0 & 1 & \beta^k \end{bmatrix} \cdot \begin{bmatrix} \frac{\partial u_0}{\partial x} \\ \frac{\partial \theta}{\partial x} \\ \frac{\partial \psi}{\partial x} \\ \gamma \\ \psi \end{bmatrix} = \mathbf{S}^k \hat{\boldsymbol{\varepsilon}} \tag{4}$$

where $\hat{\boldsymbol{\varepsilon}}$ is the generalized stain vector. This vector contains the axial elongation $\frac{\partial u_0}{\partial x}$, the pseudo-curvature $\frac{\partial \theta}{\partial x}$, the derivative of the amplitude of the zigzag function $\frac{\partial \psi}{\partial x}$, the average transverse shear strain $\gamma(\frac{\partial w_0}{\partial x} - \theta)$ and the variable ψ.

2.2. Derivation of the zigzag function ϕ^k

The zigzag function is defined within each layer as

$$\phi^k = \bar{\phi}^{k-1} + \frac{h^k \beta^k}{2} (\zeta^k + 1) \tag{5}$$

where $\bar{\phi}^{k-1}$ is the zigzag function value at the $k-1$ interface, with $\bar{\phi}^0 = \bar{\phi}^N = 0$ and $\xi^k = 2\frac{(z-z^{k-1})}{h^k} - 1$. The slope $\beta^k = \frac{\partial \phi^k}{\partial z}$ of the zigzag function within each layer is expressed as

$$\beta^k = \frac{G}{G^k} - 1 \tag{6}$$

where G is an average shear modulus that can be expressed in terms of the shear modulus (G^k) and the thickness (h^k) of each layer as

$$G = h \left[\sum_{k=1}^{N} \frac{h^k}{G^k} \right]^{-1} \tag{7}$$

For a more detailed description of the RZT for beams, the readers are referred to Tessler et al. [30].

2.3. Stresses and resultant stresses

The relation between the stresses and the strains for the kth layer is expressed in matrix form as

$$\boldsymbol{\sigma}^k = \begin{bmatrix} \sigma^k \\ \tau^k \end{bmatrix} = \begin{bmatrix} E^k & 0 \\ 0 & G^k \end{bmatrix} \cdot \begin{bmatrix} \varepsilon^k \\ \gamma^k \end{bmatrix} = \mathbf{D}^k \cdot \boldsymbol{\varepsilon}^k \tag{8}$$

where E^k, G^k and $\mathbf{D}^k$ are the Young modulus, the shear modulus and the constitutive matrix for the kth layer, respectively. The resultant stresses are computed by integrating the stresses over the beam section with area A as

$$\hat{\boldsymbol{\sigma}} = \int_A \mathbf{S}^k \boldsymbol{\sigma}^k dA \tag{9}$$

2.4. LRZ beam element

The kinematics variables of Eq. (2) are discretized using 2-noded C^0 beam elements of length l^e as

$$\mathbf{a} = \begin{bmatrix} u_0 \\ w_0 \\ \theta \\ \psi \end{bmatrix} = \sum_{i=1}^{2} \mathbf{N}_i \cdot \mathbf{a}_i^{(e)} = \mathbf{N} \cdot \mathbf{a}^{(e)} \tag{10}$$

with

$$\mathbf{N}_i = N_i \mathbf{I}_4 \text{ and } \mathbf{a}_i^{(e)} = \begin{bmatrix} u_{0i} & w_{0i} & \theta_i & \psi_i \end{bmatrix}^T$$

being N_i the linear C^0 continuous shape function of node ith.

The generalized strains $\hat{\boldsymbol{\varepsilon}}$ of Eq. (4) are expressed in term of the nodal degrees of freedom (DOF) using Eq. (10) as

$$\hat{\boldsymbol{\varepsilon}} = \begin{bmatrix} \frac{\partial u_0}{\partial x} \\ \frac{\partial \theta}{\partial x} \\ \frac{\partial \psi}{\partial x} \\ \gamma \\ \psi \end{bmatrix} = \sum_{i=1}^{2} \begin{bmatrix} \frac{\partial N_i}{\partial x} u_{0i} \\ \frac{\partial N_i}{\partial x} \theta_i \\ \frac{\partial N_i}{\partial x} \psi_i \\ N_i \gamma_i \\ N_i \psi_i \end{bmatrix} = \sum_{i=1}^{2} \mathbf{B}_i \cdot \mathbf{a}_i^{(e)} = \mathbf{B} \cdot \mathbf{a}^{(e)} \tag{11}$$

being $\mathbf{B}_i$ the generalized strain matrix defined as

$$\mathbf{B}_i = \begin{bmatrix} \frac{\partial N_i}{\partial x} & 0 & 0 & 0 \\ 0 & 0 & \frac{\partial N_i}{\partial x} & 0 \\ 0 & 0 & 0 & \frac{\partial N_i}{\partial x} \\ 0 & \frac{\partial N_i}{\partial x} & -N_i & 0 \\ 0 & 0 & 0 & N_i \end{bmatrix} \tag{12}$$

Using the virtual work principle and Eqs. (8), (9), and (11), we can obtain the element stiffness matrix $\mathbf{K}^e$ and the equivalent nodal forces $\mathbf{F}^e$ for the LRZ linear beam elements as

$$\mathbf{K}^e = \int_l \mathbf{B}^T \hat{\mathbf{D}} \mathbf{B} dl; \quad \mathbf{F}^e = \int_l N_i q[1, 0, 0, 0]^T dl \tag{13}$$

where l is the element length, q is the distributive load and $\hat{\mathbf{D}}$ is the constitutive generalized matrix defined as

$$\hat{\mathbf{D}} = \int_A [\mathbf{S}^k]^T \mathbf{D}^k \mathbf{S}^k dA \tag{14}$$

Full integration of matrix $\mathbf{K}^e$ requires a two-point Gauss quadrature. This however leads to shear locking for slender beams. This problem is eliminated by using reduced integration (one-point Gauss quadrature) for all term of $\mathbf{K}^e$ [1].

Details of the formulation of the 2-noded LRZ beam element can be found in [1].

3. Isotropic damage model

The non-linear behavior of material is modeled with an isotropic damage model [2] in which the level of damage or degradation is monitored through a single internal scalar variable d. This variable takes values ranged between 0 (no damage) and 1 (full damage). The constitutive equation for this model is defined as

$$\boldsymbol{\sigma} = (1-d)\boldsymbol{\sigma}_0 = (1-d)\mathbf{D}_0 \cdot \boldsymbol{\varepsilon} \tag{14}$$

where $\boldsymbol{\sigma}$ and $\boldsymbol{\varepsilon}$ are the stress and strain tensors, respectively, and $\mathbf{D}_0$ is the undamaged constitutive tensor. In order to distinguish between a damage state and an undamaged one, it is necessary to define a damage criterion which is formulated here in the undamaged stress space as

$$F(\boldsymbol{\sigma}_0, d) = f(\boldsymbol{\sigma}_0) - c(d) \leqslant 0 \tag{15}$$

where $f(\boldsymbol{\sigma}_0)$ is a norm used to compare different states of deformation and $c(d)$ is the damage threshold. Damage occurs when the value of $f(\boldsymbol{\sigma}_0)$ is larger than $c(d)$. Damage starts for $f(\boldsymbol{\sigma}_0) > c_0$, being c_0 the initial damage threshold value which depends on the material properties. In our work we have defined c_0 as

$$c_0 = \frac{f_t}{\sqrt{E_0}} \tag{16}$$

where f_t is the tensile strength and E_0 the Young modulus of the undamaged material.

The norm chosen in this work is defined as

$$f(\boldsymbol{\sigma}_0) = \sqrt{\boldsymbol{\varepsilon} : \boldsymbol{\sigma}_0} \tag{17}$$

The evolution law for the damage threshold and the damage variable d is obtained using the damage consistency parameter according to the Kuhn–Tucker conditions. The evolution of these variables can be explicitly integrated [34] to obtain
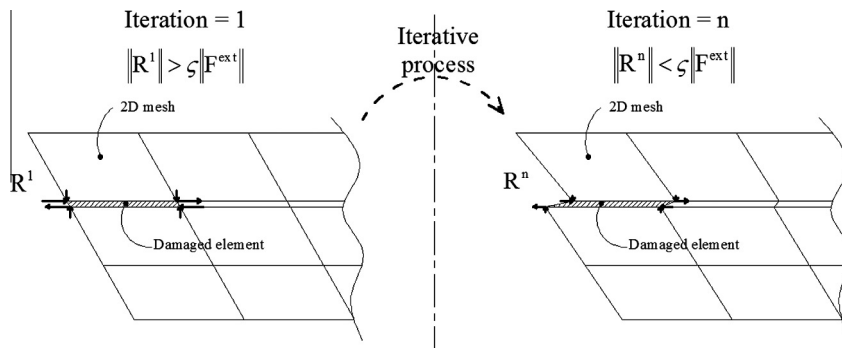

Fig. 1. The delaminated displacement field is achieved by the residual forces (R) in a plane stress analysis (PS).
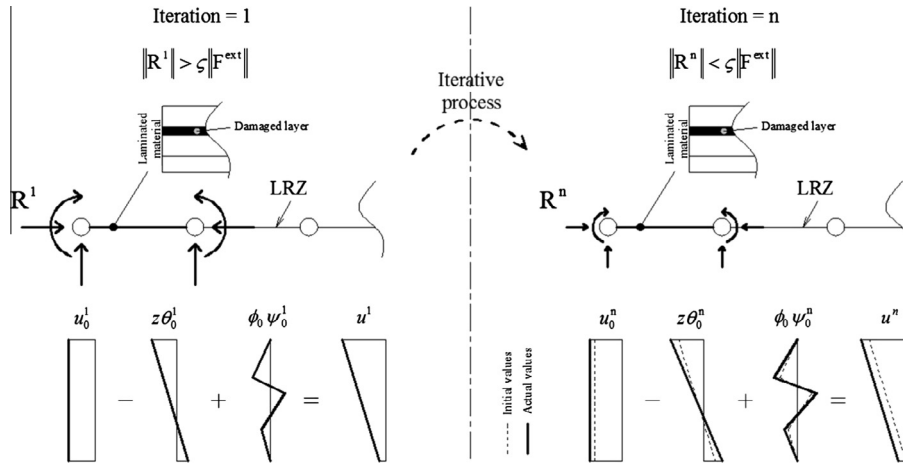
Fig. 2. The residual forces are not capable to induce delamination when the zigzag function ϕ^k is not updated.

$$d = G(f(\boldsymbol{\sigma}_0))$$
$$c(d) = \max\{c_0; \max\{f(\boldsymbol{\sigma}_0)\}\} \tag{18}$$

where $G(\bullet)$ is a monotonic scalar function ranging between 0 and 1 which defines the evolution of the damage variable. In this work an exponential evolution law is adopted for G as

$$G(f(\boldsymbol{\sigma}_0)) = 1 - \frac{f^0(\boldsymbol{\sigma}_0)}{f(\boldsymbol{\sigma}_0)} e^{B\left(1 - \frac{f(\boldsymbol{\sigma}_0)}{f^0(\boldsymbol{\sigma}_0)}\right)} \text{ with } f^0(\boldsymbol{\sigma}_0) = c_0 \tag{19}$$

Considering the norm of Eq. (17), the exponential softening of Eq. (19), and the initial damage threshold value c_0 (Eq. (16)), the parameter B is computed as

$$B = \left(\frac{G_f \cdot E_0}{l^* \cdot (f_t)^2} - \frac{1}{2}\right)^{-1} \geqslant 0 \tag{20}$$

being G_f the fracture energy per unit area and l^* a characteristic length. In this paper, l^* is equal to the influence of each Gauss point.

4. Algorithm for the non-linear solution

When a degradation process is considered in the constitutive material model it is necessary to solve a non-linear system of algebraic equations of the form

$$\mathbf{F}^{ext} - \mathbf{F}^{int}(\mathbf{q}) = \mathbf{R}(\mathbf{q}) \tag{21}$$

being $\mathbf{q}$ the discretization parameters, $\mathbf{F}^{ext}$ and $\mathbf{F}^{int}(\mathbf{q})$ the external and internal forces, respectively, and $\mathbf{R}(\mathbf{q})$ the residual vector. Note, that the dynamic forces are not considered in this work. In this work, the modified Newton–Raphson method is adopted to solve the nonlinear equation system of Eq. (21). Hence, the following linear problem is solved for each iteration

$$d\mathbf{q} = (^{i-1}\mathbf{K}_S)^{-1}{}^{i-1}\mathbf{R} \tag{22}$$

where $d\mathbf{q}$ is the increment of the nodal DOFs at ith iteration. Note that both the damaged stiffness matrix $\mathbf{K}_S$ and the residual vector $\mathbf{R}$ were computed at the previous $i-1$th iteration. For the LRZ element the matrix $\mathbf{K}_S$ is defined as

$$^{i-1}\mathbf{K}_S = \int_l \mathbf{B}^{T\,i-1}\widehat{\mathbf{D}}_S \mathbf{B}\, dl \tag{23}$$

with

$$^{i-1}\widehat{\mathbf{D}}_S = \int_A \left[^{i-1}\mathbf{S}^k\right]^{T\,i-1}\mathbf{D}_S^{k\,i-1}\mathbf{S}^k dA \text{ and } ^{i-1}\mathbf{D}_S^k = \left(1 - ^{i-1}d^k\right)\mathbf{D}_0^k \tag{24}$$

The updated DOFs are obtained as

$$^i\mathbf{q} = ^{i-1}\mathbf{q} + d\mathbf{q} \tag{25}$$

This process is repeated until the convergence criterion $\|\mathbf{R}\| \leqslant \varsigma\|\mathbf{F}\|$ is satisfied [35] where ς is a predefined error tolerance.

In 2D finite element analysis, the nodal DOFs $\mathbf{q}$ are the Cartesian displacements $\mathbf{a} = [u_x \quad u_y \quad u_z]$. According to these variables, the
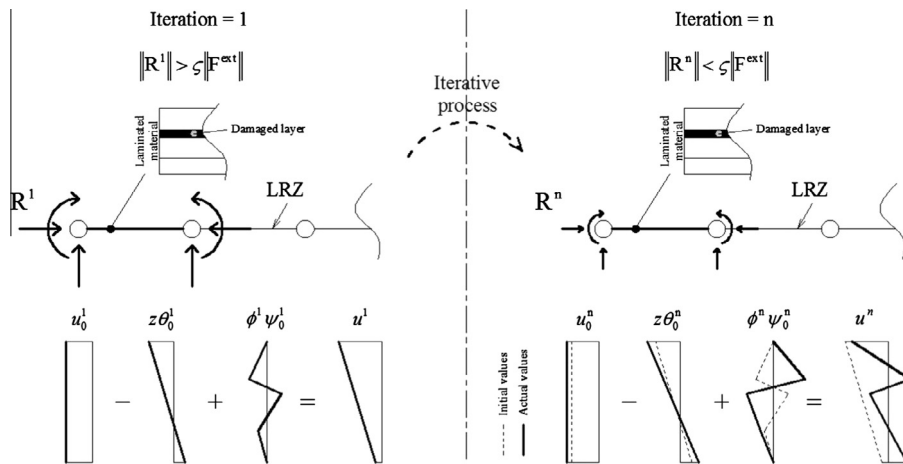

Fig. 3. Delamination can be captured with the LRZ finite element when the zigzag function ϕ^k is updated by reducing the shear modulus of the damaged layer.

Loop over load increments

    Update external forces $\mathbf{F}^{\text{ext}}$

    # **Iterative process**

        If ith iteration = 1

$$^{1}\mathbf{a} = \mathbf{K}_S^{-1} \cdot \mathbf{F}^{\text{ext}}$$

$$^{1}\boldsymbol{\varepsilon}^k = \mathbf{S}^k \, \mathbf{B} \, ^{1}\mathbf{a}$$

Note that for the first iteration both $\mathbf{K}_S^{-1}$ and $\mathbf{S}^k$ were computed at the last iteration of the previous load increment.

        Else

$$^{i}d\mathbf{a} = {}^{i-1}\mathbf{K}_S \cdot {}^{i-1}\mathbf{R}$$

$$^{i}\mathbf{a} = {}^{i-1}\mathbf{a} + {}^{i}d\mathbf{a}$$

$$^{i}\boldsymbol{\varepsilon}^k = {}^{i-1}\mathbf{S}^k \, \mathbf{B} \, ^{i}\mathbf{a}$$

Remember that $^{i-1}\mathbf{S}^k$ contains $^{i-1}\phi^k$ and $^{i-1}\tilde{\beta}^k$ computed at the previous iteration.

        End if

Evaluate undamaged stresses

$$^{i}\boldsymbol{\sigma}_0^k = \mathbf{D}_0^k \cdot {}^{i}\boldsymbol{\varepsilon}^k$$

Update damage variable:

$$^{i}d^k = 1 - \frac{c_0}{^{i}f} e^{A\left(1 - \frac{^{i}f}{c_0}\right)}$$

Update stresses and shear modulus:

$$^{i}\boldsymbol{\sigma}^k = \left(1 - {}^{i}d^k\right) {}^{i}\boldsymbol{\sigma}_0^k$$

$$^{i}\tilde{G}^k = \left(1 - {}^{i}d^k\right) {}^{i}G_0^k$$

Update zigzag function:

$$^{i}\tilde{G} = h\left[\sum_{k=1}^{N} \frac{h^k}{^{i}\tilde{G}^k}\right]^{-1}$$

$$^{i}\tilde{\beta}^k = \frac{^{i}\tilde{G}}{^{i}\tilde{G}^k} - 1$$

$$^{i}\phi^k = \bar{\phi}^{k-1} + \frac{h^k \, {}^{i}\tilde{\beta}^k}{2}\left(\zeta^k + 1\right)$$

Computation of the secant stiffness matrix and internal forces:

$$^{i}\mathbf{K}_S = \int_l \mathbf{B}^T \, {}^{i}\hat{\mathbf{D}}_S \, \mathbf{B} \, dl$$

$$^{i}\mathbf{F}^{\text{int}} = \int_V \mathbf{B}^T \, {}^{i}\mathbf{S}^T \, {}^{i}\boldsymbol{\sigma}^k \, dV$$

Verification of convergence criteria

$$\mathbf{F}^{\text{ext}} - {}^{i}\mathbf{F}^{\text{int}} = {}^{i}\mathbf{R}$$

$$\left\|^{i}\mathbf{R}\right\| \leq \varsigma \left\|\mathbf{F}^{\text{ext}}\right\|$$

    # **END iterative process**
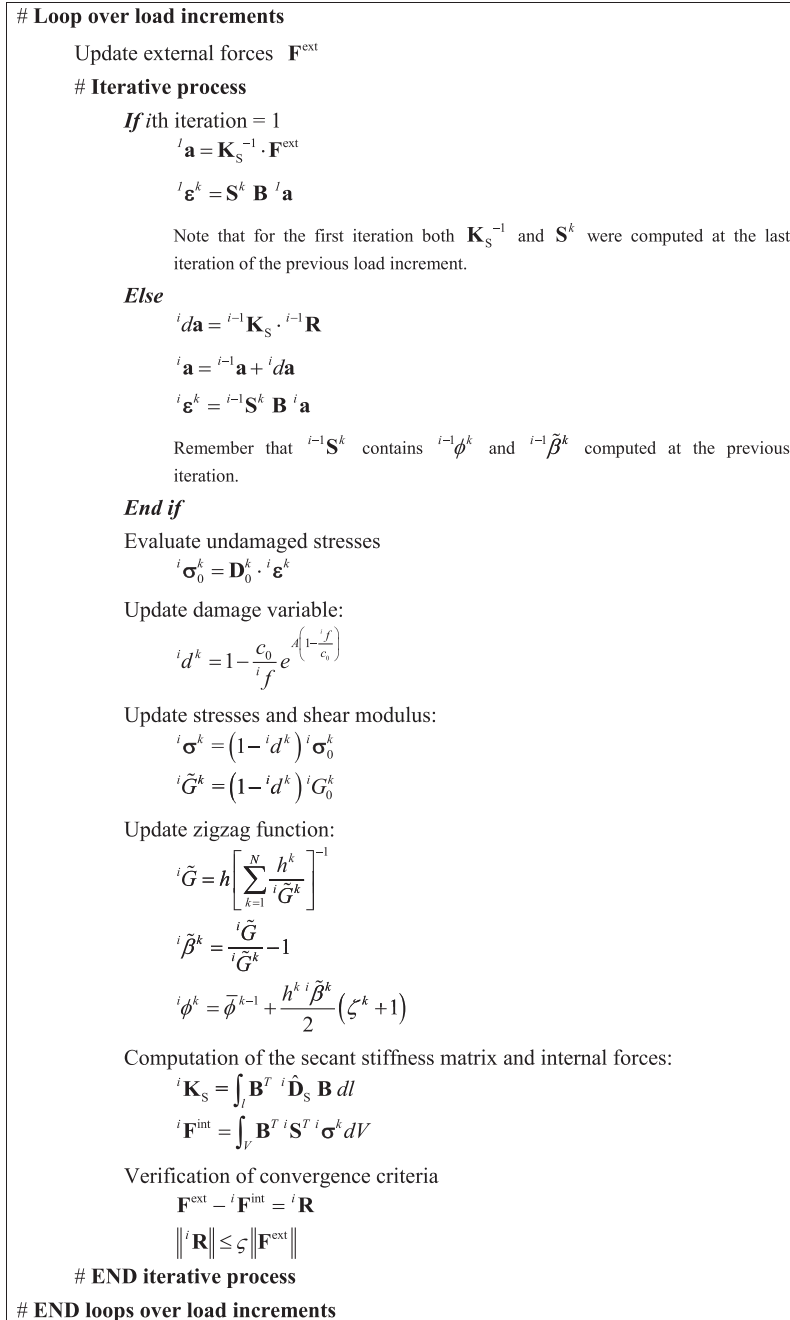
END loops over load increments

Fig. 4. Algorithm for solving the non-linear problem using the modified Newton–Raphson method. Note that the zigzag function is updated at each iteration.

stress resultants obtained by integrating the stresses on the finite element volume are three forces that induce the movement of the node. So, when a finite element starts to suffer softening
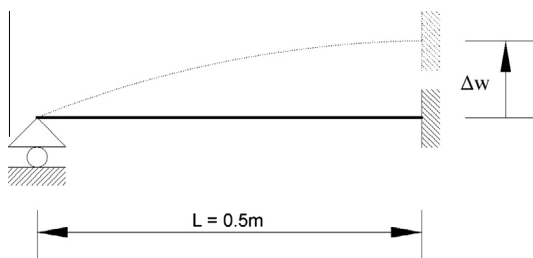

Fig. 5. Boundary conditions of the analyzed beam.

($d > 0$) and its stresses are reduced by Eq. (14), a lack of equilibrium between the external and the internal forces appears which induces residual forces via Eq. (21). These residual forces applied at the nodes of a damaged 2D element generate the relative displacement between layers that occurs during a delamination process. The equilibrium displacement field is achieved using an iterative process such as that of Eqs. (22) and (25). This process is schematized in Fig. 1.

While in 3D finite element analysis, it is possible to generate the relative displacement simply using the residual forces, in the LRZ finite element it is not.

In the LRZ element, the reference surface where the kinematics variables (Eq. (2)) are computed is the middle surface ($z = 0$) of the laminate. The stress resultants computed by integrating the stresses across the beam thickness (Eq. (9)) lead to forces and moments

Table 1
Mechanical properties of linear-elastic layers.

Materials	Young's modulus (E_0)	Shear modulus (G_0)
Mechanical properties of linear-elastic plies (MPa)		
A	157.9×10^4	5.93×10^4
B	104.0×10^1	4.00×10^2
C	5.3×10^1	2.12×10^1
D	2.19×10^1	0.876×10^1
E	0.82×10^1	0.328×10^1
F	0.73×10^{-1}	0.29×10^{-1}
G	7.3×10^1	2.92×10^1

Table 2
Mechanical properties of cohesive layers (cl).

Materials	Young's modulus (E_0) (MPa)	Shear modulus (G_0) (MPa)	Tensile strength (f_t) (MPa)	Fracture energy (G_f) (kN/m)	
				Ductile (G_f^D)	Fragile (G_f^F)
Mechanical properties of cohesive plies (cl)					
H^{cl}	104.0×10^1	4.0×10^2	6.5	5.0×10^4	1.0×10^{-2}
I^{cl}	0.73×10^{-1}	0.29×10^{-1}	0.02	5.0×10^4	1.0×10^{-3}

Table 3
Layer distribution of laminated materials.

Laminate	Layer distribution	h^k/h	h (mm)
Laminated materials			
L1	(A/B/A/H^{cl}/A/B/A/ B/A)	(0.11/0.11/0.11/0.01/0.22/0.11/ 0.11/0.11/0.11)	9.1
L2	(C/D/E/F/C/I^{cl}/G/E/ D/G)	(1.0/0.12/0.1/0.08/0.14/0.02/0.08/ 0.1/0.06/0.2)	25.0

applied at the beam element nodes on the reference surface. Consequently, there are no forces within the laminate capable of producing the relative displacement between plies. For this reason, in the RZT theory, the reduced value of stresses by Eq. (14) in an iterative process gives as result an amplification of the initial kinematics of the laminate, instead of an update of the delamination kinematics. That is so, because the variables of Eq. (2) are not capable to modify by themselves the zigzag form of the axial displacement, but they can only vary the scale of the original zigzag distribution. Fig. 2 outlines the above-mentioned problem.

In summary, the form of the zigzag axial displacement is governed by the zigzag function ϕ^k (Eq. (5)). Therefore, in order to modify the zigzag form of the laminated kinematics (Eq. (1a)) during a delamination process, it is essential to update function ϕ^k depending on the value of damage variable d. Since ϕ^k depends on the shear modulus, the update of ϕ^k is obtained by reducing the initial elastic shear modulus G_0^k at the damaged layer k by

$$\widetilde{G}^k = (1 - d^k)G_0^k \tag{26}$$

Thus, function ϕ^k is expressed in term of the damaged shear modulus as

$$\phi^k = \bar{\phi}^{k-1} + \frac{h^k \tilde{\beta}^k}{2}(\zeta^k + 1) \tag{27}$$

with

$$\tilde{\beta}^k = \frac{\widetilde{G}}{\widetilde{G}^k} - 1 \text{ and } \widetilde{G} = h\left[\sum_{k=1}^{N}\frac{h^k}{\widetilde{G}^k}\right]^{-1} \tag{28}$$

This simple but effective update of the zigzag function ϕ^k allows us to capture the relative displacement between two layers in a delamination process. A scheme of this process is shown in Fig. 3.

Fig. 4 shows the integration algorithm for solving Eq. (21) using the modified Newton–Raphson iterative scheme (Eqs. (22)–(25)), the isotropic damage model and the adapted zigzag function computed by Eq. (27).

5. Numerical simulations

The validity of the algorithm for capturing the relative in-plane displacement (Mode II) between layers is studied by modeling a beam of length $L = 0.5$ m supported as shown in Fig. 5. A vertical displacement Δw at the clamped support is imposed. The beam is analyzed for two laminates (L1 and L2) with properties shown in Tables 1–3.

The proposed method allows damage to occur at any layer of the laminate, so is not necessary to predefine the path of the crack. However since the objective of this work is to demonstrate the capability of the LRZ element for predicting relative displacement between layers, the interface where delamination will take place is defined at the onset of the analysis. Therefore, there is only one layer for each laminate, called "cohesive layer" (cl) henceforth (Fig. 7), whose mechanical behavior is modeled by the isotropic damage model, while the other plies are treated as linear-elastic. Consequently, delamination occurs when damage starts at the cohesive layer, which leads to a loss of its previous stiffness and induces the relative displacement between the adjacent layers to it.

In order to show the influence of the fracture energy G_f^{cl} in the delamination process, two values of this parameter (a larger one and a smaller one) are adopted for the cohesive layer in each laminate. For clarity, in the followings the largest value (G_f^D) is associated to a "ductile" material while the smallest (G_f^F) to a "fragile" material.

LRZ meshes of 2, 16, 128 finite elements are used in the analysis.

The reference solution is obtained by the plane stress analysis (PS) using 4-noded quadrilateral finite elements and the isotropic damage model presented in Section 4. The iterative process uses the modified Newton–Rhapson method explained in Section 5. The beam length, the thickness of the elastic layers and the thickness of the cohesive ply are discretized using 100, 2 and 1 finite elements, respectively. The discretization chosen leads to meshes of 1700 and 1900 4-noded quadrilateral PS elements for the lami-
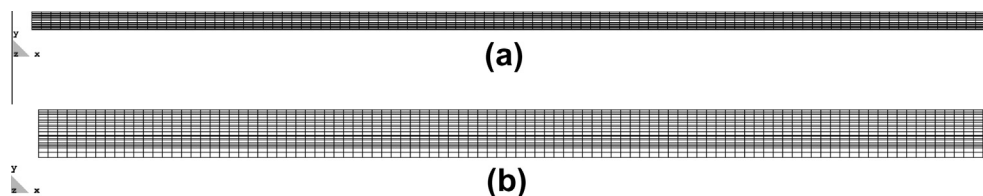

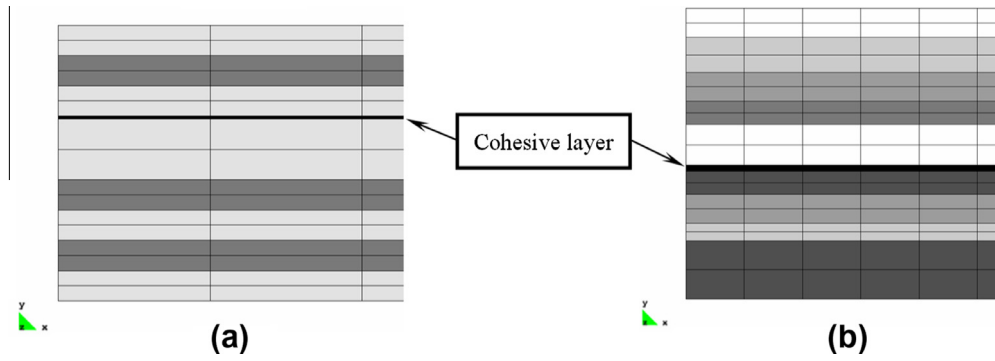**Fig. 6.** Four-noded quadrilateral finite element meshes for laminate L1 (a), and laminate L2 (b).

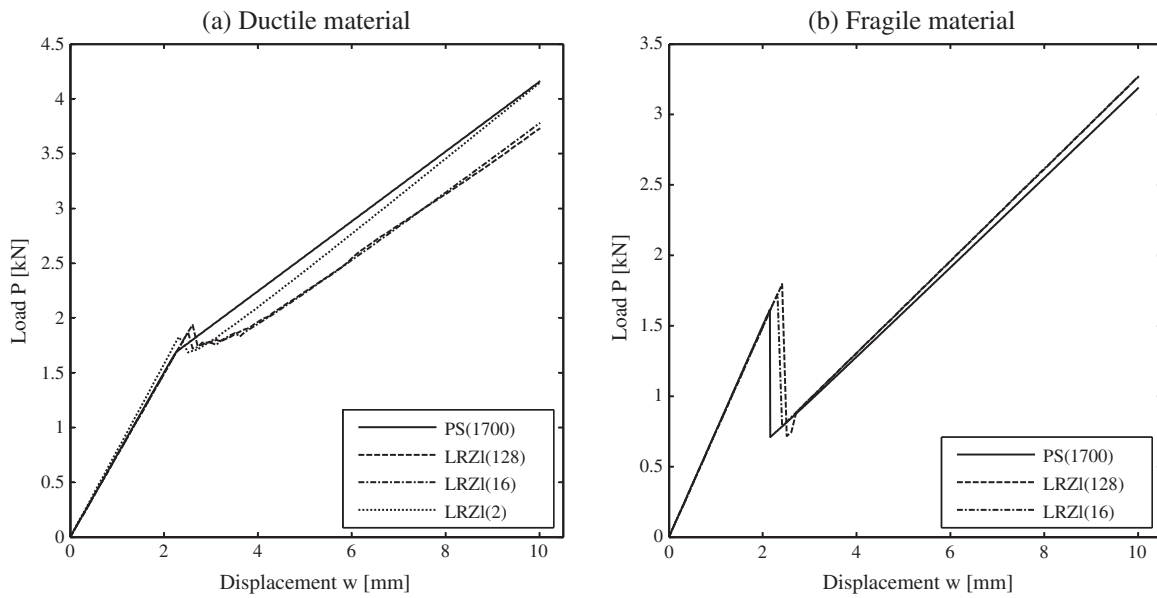**Fig. 7.** Cohesive layer in laminate L1 (a), and laminate L2 (b).

Fig. 8. Load versus displacement curves for laminate L1 with ductile (a) and fragile (b) fracture energy.
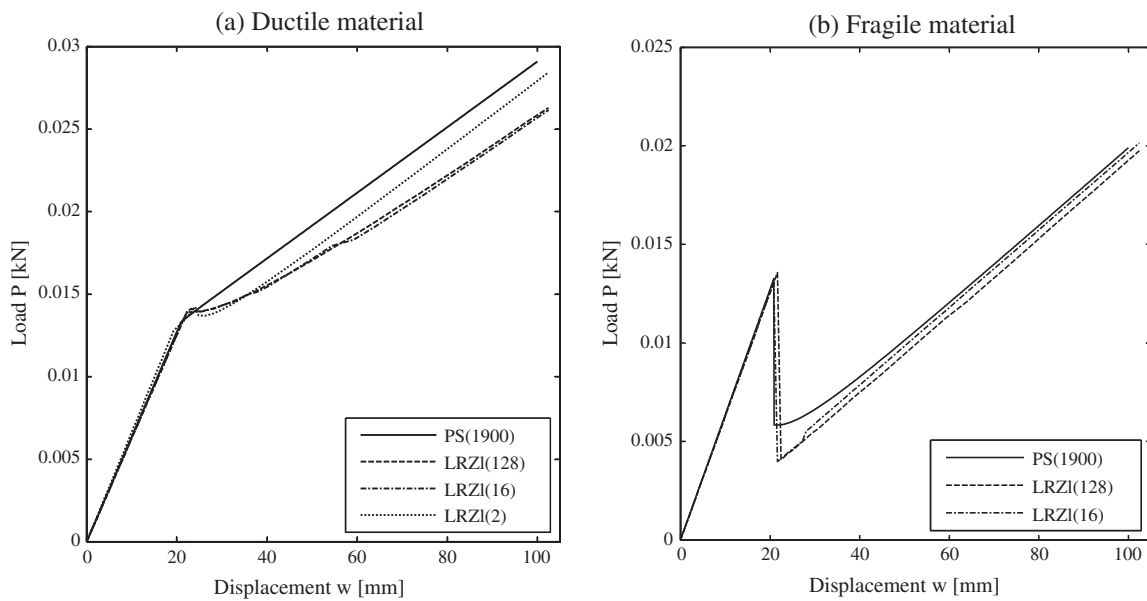

Fig. 9. Load versus displacement curves for laminate L2 with ductile (a) and fragile (b) fracture energy.

nates L1 and L2, respectively. The 2D meshes for each laminate are shown in Figs. 6 and 7.

The simulation is made under the following considerations: quasi-static application of vertical displacement at the clamped support, geometrically linear problem and small deformation.

Figs. 8 and 9 show the load–displacement graph for the laminates L1 and L2, respectively, where the curves are obtained by the PS analysis and the LRZ beam element. The load corresponds to the vertical reaction at the clamped support. The displacement corresponds to the incremental displacement Δw applied to the clamped support (Fig. 5). The curves shown in Figures a are obtained when the "ductile" (G_f^D) fracture energy is considered. The response of the beam when the "fragile" (G_f^F) fracture energy is used is shown in Figures b. The fracture energy values are noted in Table 2.

The results reveal an admissible agreement between the results obtained using PS analysis and LRZ beam elements. The errors for the finest LRZ meshes, at the end of simulation, for the cases L1-G_f^D (Fig. 8a), L1-G_f^F (Fig. 8b), $L2 - G_f^D$ (Fig. 9a) and $L2 - G_f^F$ (Fig. 9b) are less than 11.0%, 2.5%, 7.5% and 2.9%, respectively. The LRZ solution exhibits small drops of load for the case $L1 - G_f^D$ (Fig. 8a), which are not present in the PS solution. The cause of each drop is that the cohesive layer of some finite elements is totally damage at the same increment, which produces a discontinuous loss of stiffness during the simulation. The number of simultaneously delaminated elements, involved on each drop, depends on the longitudinal distribution of the transverse shear stress of the cohesive layer.

When the "fragile" value of the fracture energy (G_f^F) is used, the cohesive layer completely loses its energy at the delamination onset, which provokes the sharp drop in the sample resistance, as shown in Figures b. The loss of resistance computed by the PS solution is around 56% for both laminates, while the LRZ solution gives 60% and 70% for L1 and L2, respectively.

In all cases, both the initial stiffness and the stiffness once delamination process has started are very close to the stiffness obtained by 2D analysis. Also, is shown that delamination starts for the same values of displacement and load.
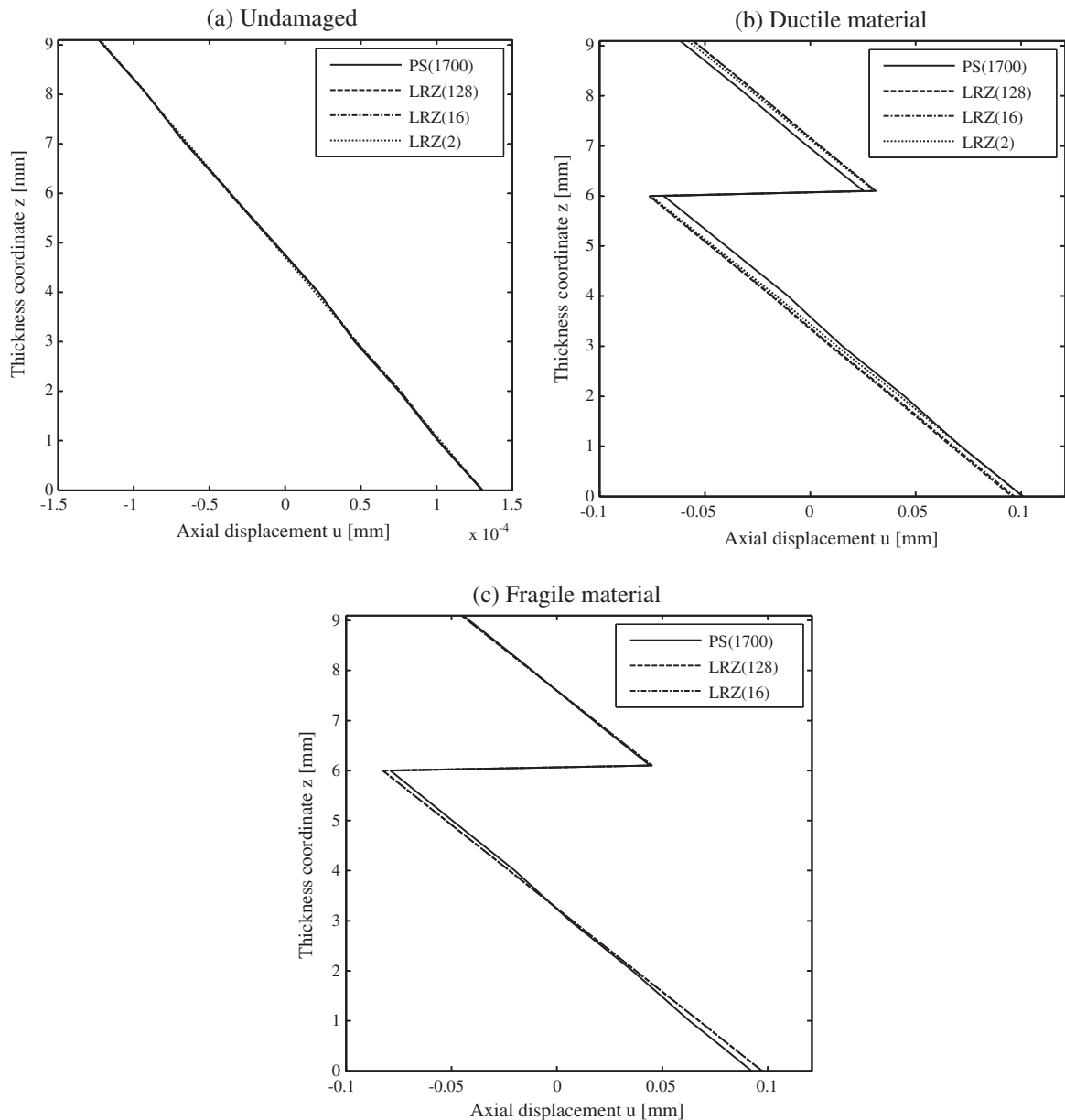

Fig. 10. Thickness distribution of the axial displacement u at the simply supported end for laminate L1. This Fig. shows the undamaged kinematics (a) and the damaged kinematics when the "ductile" (b) and the "fragile" (c) fracture energy is used.

The thickness distribution of the axial displacement u at the simply supported end, before and after delamination onset, is shown in Figs. 10 and 11 for laminates L1 and L2, respectively.

The undamaged kinematics is shown in Figures a, in which the very good match between PS and LRZ kinematics is evident.

Figs. 10 and 11b and c show the delaminated kinematics at the end of simulation when the "ductile" and the "fragile" fracture energy values are used, respectively. In the "ductile" case (Figures b), the LRZ elements are capable to capture the relative displacement with errors around 11% and 16% for laminates L1 and L2, respectively. In the "fragile" case (Figures c), the errors are less than 3.3% for both laminates.

Almost identical results are obtained with the quadratic LRZ beam element.

Fig. 12 shows the thickness distribution of the zigzag function ϕ for laminate L1 (Fig. 12a) and laminate L2 (Fig. 12b). The solid line represents the initial zigzag function (undamaged), whereas that the dashed line and the dash-dot line correspond to the damaged zigzag function when the damage variable of cohesive layer is equal to 0.9 and 1, respectively. As is mentioned in Section 5, the ability of the LRZ element to capture the relative displacement between plies during a delamination process lies in updating the zigzag function as the layers are damaged.

In order to compare the performance of the PS and the LRZ analyses, both the total increment numbers and incremental displacement values as well as the tolerance value ($\varsigma = 1 \times 10^{-4}$) are the same for both methods. The total increment numbers are equal to 1000 and 7000 for laminates L1 and L2, respectively. The incremental displacement value applied in each increment is 1×10^{-3} mm and 4×10^{-3} mm for L1 and L2, respectively. Tables 4 and 5 show the total number of iterations, the maximum number of iteration needed for achieving convergence in any increment and the total CPU time used in the simulation for L1 and L2, respectively.

As expected, the computation time needed for the PS analysis is several times greater than that required for the LRZ solutions.
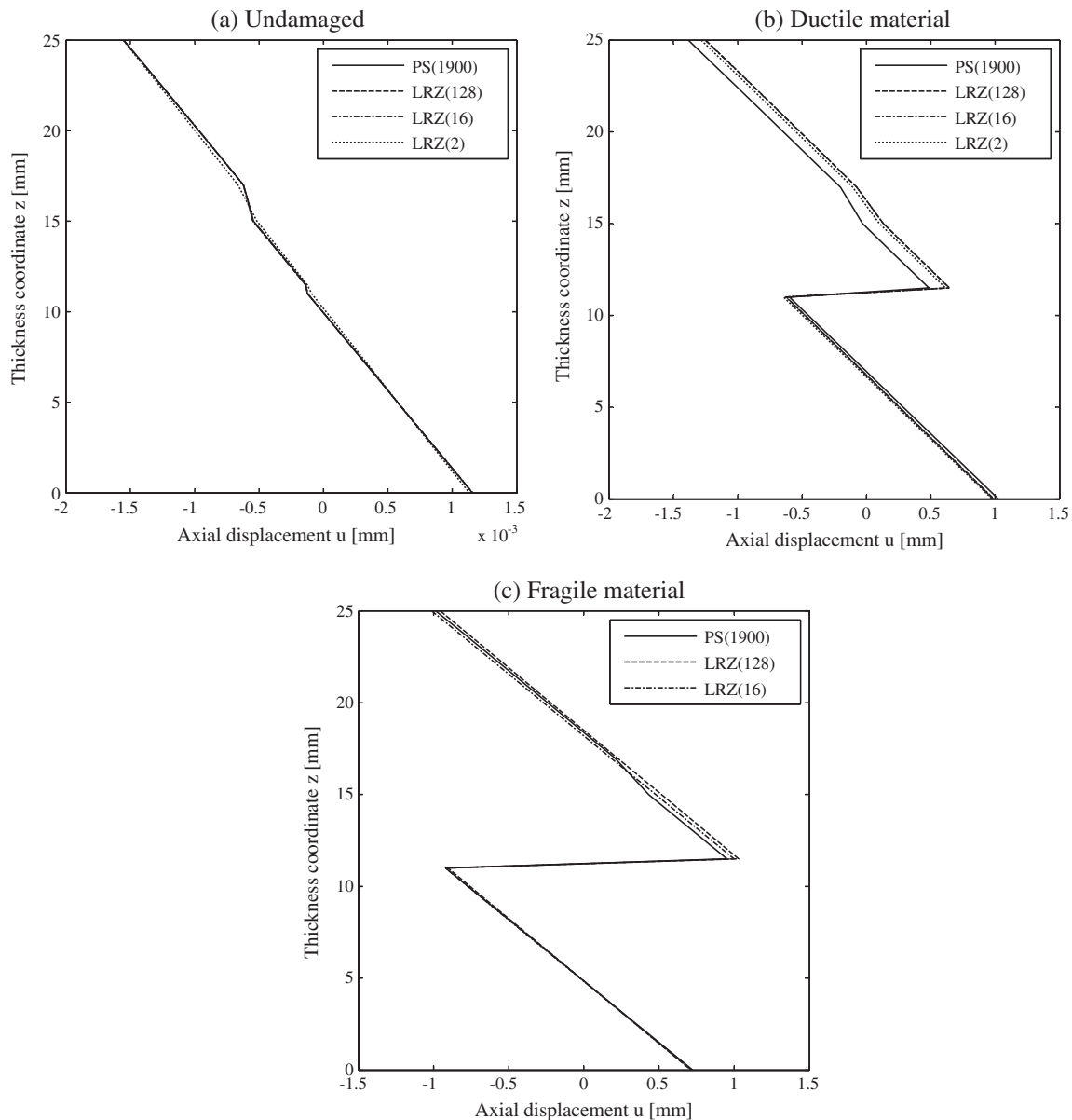

Fig. 11. Thickness distribution of the axial displacement u at the simply supported end for laminate L2. This Fig. shows the undamaged kinematics (a) and the damaged kinematics when the "ductile" (b) and the "fragile" (c) fracture energy is used.
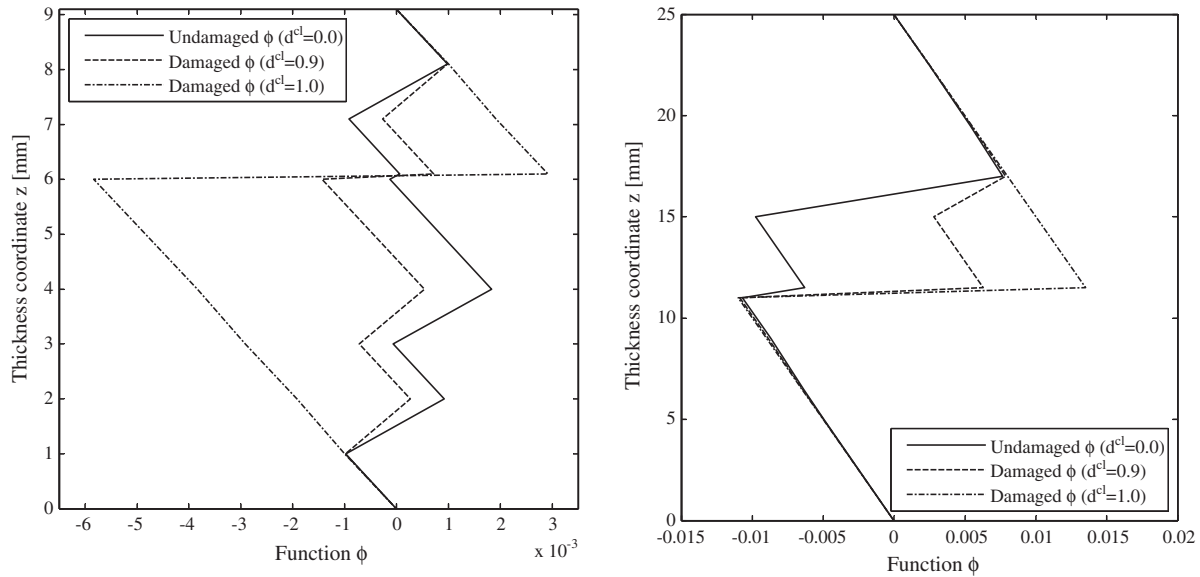
Fig. 12. Undamaged and damaged zigzag function for laminate L1 (a) and laminate L2 (b).

Table 4
Computational cost of the iterative process for laminate L1.

Finite elements		$G_f^D = 5.0 \times 10^4$ (Ductile)			$G_f^F = 1.0 \times 10^{-2}$ (Fragile)		
		Total iter.	Max. iter.	Time (seg)	Total iter.	Max. iter.	Time (seg)
Computational cost of the iterative process for laminate L1							
2D	1700	9308	485	3069.0	3465	254	1127.0
LRZ	2	1543	166	1.52	–	–	–
	16	1286	81	1.57	1009	9	1.27
	128	2291	225	19.61	1036	23	9.45

Table 5
Computational cost of the iterative process for laminate L2.

Finite elements		$G_f^D = 5.0 \times 10^4$ (Ductile)			$G_f^F = 1.0 \times 10^{-3}$ (Fragile)		
		Total iter.	Max. iter.	Time (seg)	Total iter.	Max. iter.	Time (seg)
Computational cost of the iterative process for laminate L2							
2D	1900	18,374	88	6967.0	10,141	144	4223.0
LRZ	2	7298	76	8.10	–	–	–
	16	7131	53	8.11	7016	11	7.96
	128	7072	71	64.51	7372	101	65.46

Comparing with the finest 128-LRZ mesh, PS uses at best around 67 times the time used by LRZ solution for laminate L2 and $G_f^F = 1.0 \times 10^{-3}$ (Table 5). At worst, the time used by PS is 156 times greater than that required by the LRZ solution for laminate L1 and $G_f^D = 5.0 \times 10^4$ (Table 4). If the comparison is made versus the 16-LRZ mesh, the time used by the PS solution is 530 and 1954 times of that needed by the LRZ solution at best and at worst scenarios, respectively.

6. Conclusions

We have presented a promising numerical method based on the RZT for simulating the delamination process (mode II) in laminated beams. This method uses LRZ beam elements for modeling the beam kinematic and an isotropic damage model for modeling the material behavior.

Results show that in order to capture the relative displacement between layers during delamination, the zigzag function has to be updated according as the layers are damaged. Therefore, both the stresses and the zigzag function are degraded by the damage variable during the iterative process.

The ability of this formulation to capture the relative displacement has been proved by the study of delamination in a beam for two different laminates. The comparison of the LRZ solution with the plane stress plate elements analysis revels that the technique presented is capable to predict both the onset and the propagation of delamination. Also, the updating of zigzag function has proven to be essential for reproducing the delaminated kinematics.

A comparison of the computational time between both adopted techniques has shown that, as expected, the computation time and the memory space needed by the LRZ beam element is several times less than that required by a 2D PS analysis.

The extension of the proposed formulation to plate and shells is possible since the RZT plate theory has the same basic features as the RZT beam theory. Because of the kinematics of the RZT plate theory, the extended formulation is able to model not only the fracture mode II but also the mode III. However, this methodology is unable to simulate the fracture mode I since the vertical displacement is defined constant through the thickness of the laminate.

References

[1] Oñate E, Eijo A, Oller S. Simple and accurate two-noded beam element for composite laminated beams using a refined zigzag theory. Comput Method Appl Mech Eng 2012:362–82.
[2] Oliver J, Cervera M, Oller S, Lubliner J. Isotropic damage models and smeared crack analysis of concret. In: Second international conference on computer aided analysis and design of concrete structures Zell am See, Austria; 1990.
[3] Bolotin VV. Delaminations in composite structures: its origin, buckling, growth and stability. Compos: Part B 1996;27B:129–45.

[4] Krueger R. The virtual crack closure technique: history, approach and applications. Appl Mech Rev 2002;57(2):109–43.

[5] Mabson G. Fracture analysis for bondlines and interfaces of composite structures. In: 4th International conference on composites testing and model identification (Comptest2008). Dayton (OH); 2008.

[6] Borg R, Nilsson L, Simonsson K. Modeling of delamination using a discretized cohesive zone and damage formulation. Compos Sci Technol 2002;62(10–11):1299–314.

[7] Turon A, Camanho PP, Costa J, Dávila CG. A damage model for the simulation of delamination in advanced composites under variable-mode loading. Mech Mater 2006;38(11):1072–89.

[8] Balzani C, Wagner W. An interface element for the simulation of delamination in unidirectional fiber-reinforced composite laminates. Eng Fract Mech 2008;75(9):2597–615.

[9] Turon A, Camanho PP, Costa J, Renart J. Accurate simulation of delamination growth under mixed-mode loading using cohesive elements: definition of interlaminar strengths and elastic stiffness. Compos Struct 2010;92:1857–64.

[10] Wagner W, Balzani C. Simulation of delamination in stringer stiffened fiber-reinforced composite shells. Comput Struct 2008;86(9):930–9.

[11] Martinez X, Rastellini F, Oller S, Flores F, Oñate E. Computationally optimized formulation for the simulation of composite materials and delamination failures. Compos: Part B 2011;47(–):134–44.

[12] Timoshenko SP, Woinowsky-Krieger S. Theory of plates ans shells. 3rd ed. New York: McGraw-Hill; 1959.

[13] Kirchhoff G. Über das Gleichgewicht und die Bewegung einer elastishen Scheibe. J Angew Math 1850;40:51–88.

[14] Timoshenko SP. On the correction for shear of differential equations for transverse vibrations of prismatic bars. Philos Mag Ser 1921;41:744–6.

[15] Reissner E. The effect of transverse shear deformation on the bending of elastic plates. Appl Mech 1945;12:69–79.

[16] Mindlin RD. Influence of rotatory inertia and shear in flexural motions of isotropic elastic plates. Appl Mech 1951;18:31–8.

[17] Reddy JN. A generalization of two-dimensional theories of laminated plates. Commun Appl Numer Method 1987;3(3):173–80.

[18] Reddy JN, Robbins DH. Theories and computational models for composite laminates. Appl Mech Rev 1994;47(6):147–65.

[19] Liu D, Li X. An overall view of laminate theories based on displacement hypothesis. J Compos Mater 1996;30(14):1539–61.

[20] Barbero EJ, Reddy JN. Modeling of delamination in laminates using a layer-wise plate theory. Int J Solids Struct 1991;28(3):373–88.

[21] Thornburgh R, Chattopadhyay A. Unified approach to modeling matrix cracking and delamination in laminated composite structures. AIAA 2001;39(1):153–60.

[22] Williams TO, Addessio FL. A general theory for laminated plates with delaminations. Int J Solids Struct 1997;34(16):2003–24.

[23] Hosseini-Toudeshky H, Hosseini S, Mohammadi B. Delamination buckling growth in laminated composites using layerwise-interface element. Compos Struct 2010;92(8):1846–56.

[24] Na WJ, Reddy JN. Delamination in cross-ply laminated beams using the layerwise theory. Asian J Civil Eng 2009;10:451–80.

[25] Wanji C, Zhen W. A selective review on recent development of displacement-based laminated plate theories. Recent Pat Mech Eng 2008;1:29–44.

[26] Carrera E. Historical review of Zig-Zag theories for multilayered plates and shells. Appl Mech Rev 2003;56(3):287–308.

[27] Averill RC, Yip YC. Development of simple, robust finite elements based on refined theories for thick laminated beams. Comput Struct 1996;59(3):529–46.

[28] Aitharaju VR, Averill RC. C_0 zig-zag finite element for analysis of laminated composite beams. ASCE 1999;59:502–9.

[29] Icardi U, Zardo G. C^0 plate element for delamination damage analysis, based on a zig-zag model and strain energy updating. Int J Impact Eng 2005;31(5):579–606.

[30] Tessler A, Sciuva MD, Gherlone M. A refined zigzag beam theory for composite and sandwich beams. J Compos Mater 2009;43(9):1051–81.

[31] Tessler A, Sciuva MD, Gherlone M. A consistent refinement of first-order shear deformation theory for laminated composite and sandwich plates using improved zigzag kinematics. Mech Mater Struct 2010;5(2):341–65.

[32] Tessler A, Sciuva MD, Gherlone M. Refined zigzag theory for homogeneous, laminated composite, and sandwich plates: a homogeneous limit methodology for zigzag function selection. Numer Meth Part Diff Eq 2011;27(1):208–29.

[33] Lemaitre J, Chaboche JL. Mechanics of solid materials. Cambridge: Press Syndicate of the University of Cambridge; 1990.

[34] Oller S. Fractura mecánica. Un enfoque global., 1ra ed., CIMNE, Barcelona, España; 2001 [ISBN: 84-89925-76-3].

[35] Zienkiewicz OC, Taylor RL. El método de los elementos finitos, vol. 2, 5 ed. CIMNE, Barcelona; 2004 [ISBN: 84-95999-53-6].